Research paper

Study of argon ions density and electron temperature and density in magnetron plasma by optical emission spectroscopy and collisional-radiative model

Kirill E. Evdokimov*, Maxim E. Konischev, Vladimir F. Pichugin, Z. Sun

Tomsk Polytechnic University, 30 Lenin Avenue, Tomsk, 634050, Russian Federation

A B S T R A C T

Optical emission spectroscopy (OES) combined with the models of plasma light emission becomes non-intrusive and versatile method of plasma parameters determination. In this paper we have studied the densities of charge carriers and electron temperature in Ar plasma of pulsed DC magnetron in different experimental conditions. Electron density and temperature were determined by fitting of relative emission line intensities calculated from collisional-radiative model (CRM) to experimental ones. The model describes the kinetics of the first 40 excited states of neutral argon Ar and takes into account the following processes: electron impact excitation/deexcitation, spontaneous light emission, radiation trapping, electron impact ionization, and metastable quenching due to diffusion to walls. Then, ions density was determined from relative intensity of 488 nm Ar^+ emission line and simple CRM accounting excitation from ground states of neutral Ar and ion Ar^+. The values of electron and ion density agree very well. To test the stability of results, we performed Monte-Carlo calculations with random variation of experimental spectrum as well as of excitation cross-sections and estimated confidence intervals and errors for plasma parameters. Also, we validated OES study by comparison with Langmuir probe measurements. The agreement between optical and probe techniques is satisfactory.

© 2017 Tomsk Polytechnic University. Published by Elsevier B.V. This is an open access article under the CC BY-NC-ND license. (http://creativecommons.org/licenses/by-nc-nd/4.0/)

1. Introduction

Optical emission spectroscopy (OES) is widely used for low-temperature plasma diagnostics [1–6]. This method is comparatively cheap, versatile and non-intrusive. It allows determining such plasma parameters as electron temperature and density by so-called line-ratio technique. Each spectral line corresponds to optical transition between two quantum levels of atom/molecule, and a number density of gas species in the upper state determine spectral line intensity. In its turn the number density is the function of electron temperature and density. Having determined densities of species in various states by some population model, one can calculate dependence of different spectral line intensity ratios versus electron temperature and density and distinguish these parameters by comparison with experiment.

A population model should take into account two main processes in the case of low-temperature plasma: electron impact excitation and optical radiative transition. In general such models

are called collisional-radiative and the simplest one called *corona model* takes into account only excitation and optical transition from one level [7]. For argon plasma there are some metastable states playing important role in kinetics, corona model is not valid for most states and one should use more comprehensive one. The review of usage of collisional-radiative models (CRM) for determination of plasma parameters can be found in [4].

This paper aims to study parameters of magnetron discharge plasma. We developed argon CRM, measured emission spectra of plasma in laboratory installation for reactive magnetron sputter deposition and proposed technique for determination of electron temperature and density by minimization of merit function composed from experimental and model line intensities. Also, we compared determined electron parameters with the results of double Langmuir probe measurements and Ar ions density calculated from simple CRM for Ar^+.

2. Experiment

Plasma of magnetron discharge in laboratory installation UVN-200MI with pulsed DC magnetron for reactive sputter deposition

* Corresponding author.
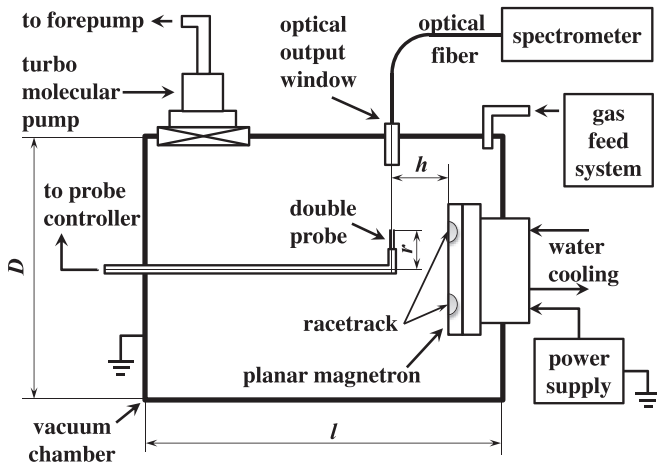 *E-mail address:* evdokimov@tpu.ru (K.E. Evdokimov).

Fig. 1. Sketch of the experimental setup: $D = 380$ mm is the vacuum chamber diameter, $l = 450$ mm is chamber length, $h = 100$ mm is the distance between magnetron plane and optical window axis, $r = 65$ mm is the distance between chamber axis and the probe tips.

Fig. 2. Emission spectrum of Ar plasma in laboratory installation UVN-200MI for reactive magnetron sputter deposition. Most intense lines of Ar atom are marked by corresponding wavelength. Operation parameters: discharge power 1 kW, pressure 0.06 Pa.

was investigated. [8]. Cylindrical vacuum chamber of the installation has diameter 380 mm and length 450 mm. Vacuum pumping speed is 150 l/s and working pressure varies from 0.04 to 0.5 Pa. A titanium target with 200 mm diameter was sputtered in argon atmosphere. Magnetron power source PS MS1 provides modulated magnetron supply with frequency 60 kHz and fill factor 80%, and works in the average power stabilization regime.

Plasma emission spectra were detected by Avantes Avaspec 3648 spectrophotometer with spectral resolution (FWHM) of 1.4 nm. Optical system including spectrophotometer and optic fiber was intensity calibrated with a tungsten-ribbon lamp. Optical fiber was connected to light output window straightly without lens. Output window was protected from contamination by steel tube with 6 mm inner diameter and 42 mm length placed inside the chamber. Taking into account 18 mm thick chamber walls, the effective acceptance angle can be estimated as 6° giving the effective collecting volume of $1.5 \cdot 10^{-4}$ m^3.

Simultaneously, double probe measurements were performed. Cylindrical probe tips are made from tungsten and have 23.4 mm length and 0.5 mm diameter. The distance between the tips is 3 mm. The probe was positioned near magnetron racetrack area in front of optical output window. Overall experiment schematic is shown in Fig. 1.

Probe data was interpolated and averaged by the algorithm described in [9] and then plasma parameters were determined using technique from [10]. First, we registered 80–100 voltage–current characteristics for each experimental instance. In our case I–V curves usually have high frequency noise due to vicinity of magnetron power source frequency and the frequency of probe data acquiring controller. To diminish this effect, all I–V curves was interpolated, averaged and additionally smoothed by Savitzky–Golay filter. Then, electron temperature was determined by voltage difference between two extrema of double derivative of I–V curve. And finally, ion density was determined by fitting experimental curve to theoretical one in orbital-motion limit approximation.

We neglected the effect of surface contamination and magnetic field because sputtered material (Ti) is a conductor and magnetic field is relatively weak. An estimate of magnetic field strength in the probe region based on characteristics of magnetic system gives value about 5 mT and corresponding electron gyration radius is much larger than the probe tip radius. However, these factors may influence determined plasma parameters, especially charge carrier density.
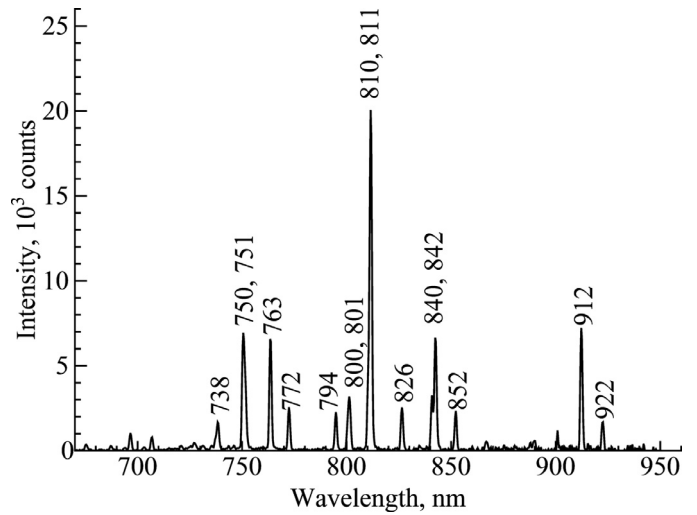
Fig. 2 represents characteristic emission spectrum of Ar plasma in the installation.

The most bright spectral lines in registered Ar emission spectrum correspond to $2p \rightarrow 1s$ transitions and lay in 660– 930 nm range where upper limit is determined by spectrophotometer sensitivity. We have chosen 20 spectral lines in this range belonging to $2p \rightarrow 1s$ manifold with Einstein coefficient exceeding 10^6 s^{-1} and determined experimental intensity I_{ij}^{OES} for each. Here indexes i and j denote the upper and the lower states of Ar atom corresponding to certain transition. Intensities of unresolved spectral lines were determined by curve-fitting method using pseudo-Voigt instrumental line shape (ILS). Parameters of ILS were derived from most bright resolved spectral lines.

3. Argon collisional-radiative model

In this work we adopted CRM proposed in Gangwar et al. [11] and extended it by taking into account metastables quenching due to collisions with vacuum chamber walls. The latter process was accounted similarly to Iordanova and Koleva [3]. CRM describes homogeneous plasma and space non-uniformity is accounted by introducing characteristic plasma length determining self-absorption and diffusion. The model considers steady-state low-temperature and low-density argon plasma and describes kinetics of ground state and first 40 excited states of Ar atom. Table 1 represents the states along with excitation energy E_i and statistical weight g_i taken from NIST Atomic Spectra Database [12]. Here, the excited states are in Paschen notation [1] and "gs" denotes the ground state.

Population of the states is determined by the following set of particle balance equations:

$$\sum_{j \neq i} n_e n_j K_{ji}^{ex} + \sum_{j > i} n_j A_{ji} \Lambda_{ji}$$
$$= n_i \sum_{j \neq i} n_e K_{ij}^{ex} + n_i \sum_{j < i} A_{ij} \Lambda_{ij} + n_e n_i K_i^{iz} + \nu_i^d n_i, \quad (1)$$

where n_e is the volume averaged electron density, n_i is the volume averaged density of atoms in ith state, K_{ij}^{ex} is the electron-impact excitation/deexcitation coefficient from ith to jth state, K_i^{iz} is the electron-impact ionization coefficient for ith state, A_{ij} and Λ_{ij} are transition probability (Einstein's coefficient) and escape fac-

Table 1
Argon energy levels considered in the model.

I	Energy level	E_i, eV	g_i
1	gs	0	1
2	$1s_5$	11.548	5
3	$1s_4$	11.624	3
4	$1s_3$	11.723	1
5	$1s_2$	11.828	3
6	$2p_{10}$	12.907	3
7	$2p_9$	13.076	7
8	$2p_8$	13.095	5
9	$2p_7$	13.153	3
10	$2p_6$	13.172	5
11	$2p_5$	13.273	1
12	$2p_4$	13.283	3
13	$2p_3$	13.302	5
14	$2p_2$	13.328	3
15	$2p_1$	13.480	1
16	$3d_{12}$	13.845	1
17	$3d_{11}$	13.864	3
18	$3d_{10}$	13.903	5
19	$3d_9$	13.979	9
20	$3d_8$	14.013	7
21	$3d_7$	14.063	5
22	$2s_5$	14.068	5
23	$2s_4$	14.090	3
24	$3d_6$	14.099	7
25	$3d_5$	14.153	3
26	$3d_4$	14.214	5
27	$3d_3$	14.234	5
28	$3d_2$	14.236	7
29	$2s_3$	14.241	1
30	$2s_2$	14.255	3
31	$3d_1$	14.304	3
32	$3p_{10}$	14.464	3
33	$3p_9$	14.499	7
34	$3p_8$	14.506	5
35	$3p_7$	14.525	3
36	$3p_6$	14.529	5
37	$3p_5$	14.576	1
38	$3p_4$	14.681	3
39	$3p_3$	14.687	3
40	$3p_2$	14.688	5
41	$3p_1$	14.738	1

Table 2
Electron-impact excitation processes considered in the model.

#	Process	Cross section reference
1	$Ar(gs)+e \leftrightarrow Ar(1s)+e$	[14]
2	$Ar(gs)+e \leftrightarrow Ar(2p)+e$	[14]
3	$Ar(gs)+e \leftrightarrow Ar(3d)+e$	[14]
4	$Ar(gs)+e \leftrightarrow Ar(2s)+e$	[14]
5	$Ar(gs)+e \leftrightarrow Ar(3p)+e$	[11]
6	$Ar(1s)+e \leftrightarrow Ar(1s)+e$	[15]
7	$Ar(1s)+e \leftrightarrow Ar(2p)+e$	[11]
8	$Ar(2p)+e \leftrightarrow Ar(2p)+e$	[11]

where $\theta_e = k_B T_e$ is the electron temperature in energy units and T_e is the electron temperature in Kelvins.

The symmetry of electron impact excitation process with respect to time inversion leads to relationship between cross-sections of excitation and deexcitation which expresses the principle of detailed balancing [13]: $g_i v_1^2 Q_{ij}(v_1) = g_j v_2^2 Q_{ji}(v_2)$, where $v_{1,2}$ are velocities of electron before and after the collision. Integration of this relation with Maxwellian distribution function yields the coefficient of deexciation from upper state j to lower state i:

$$K_{ji}^{ex} = \frac{g_i}{g_j} \, e^{\Delta E_{ij}/\theta_e} K_{ij}^{ex}. \tag{5}$$

In this work we adopted electron-impact excitation cross sections from [11,14,15]. Most of them are available on *Plasma Data Exchange Project* website (http://www.lxcat.net). The review of these and other electron-impact cross sections for Ar in terms of the project can be found in [16]. Table 2 represents considered in the model electron-impact excitation processes and references where corresponding cross sections can be found.

Other important processes affecting excited states population are the ones connected with light emission and absorption. In the model only spontaneous emission and self-absorption are taken into account. The rate of radiative decay from level i to level j equals to $n_i A_{ij} \Lambda_{ij}$; and escape factor Λ_{ij} for uniform distribution of emitting and absorbing atoms can be written as follows [17]

$$\Lambda_{ij} = \frac{2 - e^{-\rho \kappa_{ij}/1000}}{1 + \rho \kappa_{ij}}, \tag{6}$$

where ρ is the plasma characteristic length, and κ_{ij} is the reabsorption coefficient for transition $i \rightarrow j$. In case of low-temperature plasma only Doppler broadening is significant and reabsorption coefficient can be expresses as

$$\kappa_{ij} = \frac{g_i}{g_j} \frac{\lambda_{ij}^3}{8\pi^{3/2}} \, n_j A_{ij} \sqrt{\frac{M}{2\,R\,T_g}}, \tag{7}$$

where λ_{ij} is the wavelength corresponding to optical transition $i \rightarrow j$, M is the molar mass, and R is the gas constant. Wavelengths and Einstein coefficients for 133 optical transitions accounted by the model were taken from NIST database [12].

Excited atom after collision with electron can be either excited to another level or ionized. The rate of electron-impact ionization of atom in i-th state equals to $n_e n_i K_i^{iz}$ and is determined by ionization coefficient K_i^{iz} which can be expresses similarly to excitation one:

$$K_i^{iz} = \int_{E_i^{iz}}^{\infty} Q_i^{iz}(E) \, v(E) \, F(E) dE, \tag{8}$$

where Q_i^{iz} is the integral ionization cross section of atom in state i, and E_i^{iz} is corresponding ionization energy. For ionization of $1s$ states we adopted cross section calculated in [18], and for $2p$, $3d$, $2s$, $3p$ states we adopted cross sections from [19].

Inelastic collisions of excited atom with chamber walls may lead to quenching of excited state. The main transfer mechanism

tor respectively for optical transition from ith to jth state, v_i^d is the probability per unit time of quenching due to diffusion to chamber walls. Here index j runs through all 41 states listed in Table 1; index i runs through all states but ground state and the density of atoms in the ground state $n_{gs} \equiv n_1$ is determined by ideal gas law:

$$p = n_{gs} k_B T_g, \tag{2}$$

where p is the gas pressure, T_g is the volume averaged gas temperature, k_B is the Boltzmann constant.

Electron-impact excitation is one of the most important processes in the model. The rate of this process can be expressed as $n_e n_i K_{ij}^{ex}$ and depends on electron-impact excitation coefficient K_{ij}^{ex} which can be written as follows

$$K_{ij}^{ex} = \int_{\Delta E_{ij}}^{\infty} Q_{ij}^{ex}(E) \, v(E) \, F(E) dE \tag{3}$$

where Q_{ij}^{ex} is the integral electron-impact cross-section for excitation from lower state i to upper state j, $\Delta E_{ij} = (E_j - E_i)$ is the excitation energy, $v(E) = \sqrt{2E/m_e}$ is the electron velocity, m_e is the electron mass, and $F(E)$ is the electron energy distribution function (EEDF). Here EEDF is assumed to be Maxwellian and can be expresses as

$$F(E) = \frac{2}{\sqrt{\pi}} \frac{\sqrt{E}}{\theta_e^{3/2}} e^{-E/\theta_e}, \tag{4}$$

of neutrals is diffusion. The effect on population of certain level can be significant only if density of atoms in this state is high enough. Therefore, only metastable states with relatively high life-times were taken into account. In sake of generality, we introduce probability of quenching per unit time in the following way

$$
\nu_i^d = \begin{cases} (\tau_i^d)^{-1}, & \text{when } i = 2 \ (1s_5) \text{ or } i = 4 \ (1s_3); \\ 0, & \text{for other states}. \end{cases} \tag{9}
$$

where $\tau_i^d = (\rho/2405)^2/D_i$ is the characteristic time of diffusion of excited atom in i-th state, and D_i is the diffusion coefficient. According to [20] diffusion coefficients of Ar metastables at standard conditions ($T_0 = 300$ K) are given by the following: $Dn_{1s5} = 1.8 \times 10^{20}$ m^{-1}s^{-1}, $Dn_{1s3} = 1.9 \times 10^{20}$ m^{-1}s^{-1}, where Dn is the diffusion coefficient multiplied by gas density, and index denotes atom state. Taking into account the dependence of Dn on temperature, diffusion coefficient D_i can be expresses as follows

$$
D_i = \frac{Dn_i}{n_g} \sqrt{\frac{T_g}{T_0}}. \tag{10}
$$

Eqs. (1) and (2) represent system of non-linear algebraic equations with n_i, p, T_g, ρ, θ_e, and n_e as independent variables. Assuming p, T_g, ρ, θ_e, and n_e as known parameters the system can be numerically solved for excited states population densities n_i.

4. Plasma parameters determination technique

Having calculated excited states population densities, one can evaluate intensity of spectral line corresponding to optical transition $i \to j$ in the following way

$$
I_{ij}^{CRM} = C \frac{hc}{\lambda_{ij}} n_i A_{ij} \Lambda_{ij} \tag{11}
$$

where coefficient C is the same for all lines. The straight comparison between theoretical I_{ij}^{CRM} and experimental I_{ij}^{OES} intensities is not possible in our case, because space distribution of light sources is unknown. For determination of plasma parameters we employed technique similar to one used in [6].

Let us introduce relative intensities as follows

$$
I_{ij}^{RO} = \frac{I_{ij}^{OES}}{\sum_{i'j'} I_{t'j'}^{OES}}, \quad I_{ij}^{RM} = \frac{I_{ij}^{CRM}}{\sum_{i'j'} I_{t'j'}^{CRM}}, \tag{12}
$$

where indexes runs through all values corresponding spectral lines in considered wavelength range. Merit function Δ describing difference between experimental and theoretical spectrum can be introduced in following way

$$
\Delta = \sqrt{\sum_{ij} \left(I_{ij}^{RO} - I_{ij}^{RM} \right)^2}, \tag{13}
$$

where summation is done over chosen 20 spectral lines in 660–930 nm range belonging to $2p \to 1s$ manifold with Einstein coefficient exceeding 10^6 s^{-1}. For a given experimental spectrum the merit Δ is a function of p, T_g, ρ, θ_e, and n_e. Being one of the experiment control parameters, gas pressure p is assumed to be known. Minimization of merit function Δ gives values of variables T_g, ρ, θ_e, and n_e. An example of this calculation done by Wolfram Mathematica 10 code is shown in Fig. 3.

5. Argon ion density determination

For determination of Ar ion density we have chosen one of the most bright 488 nm Ar$^+$ emission line corresponding to transition from $3s^2 3p^4(^3P)4p \ ^2D^\circ_{5/2}$ state of Ar$^+$ ion. This state can be populated by straight excitation from ground state of neutral Ar as well
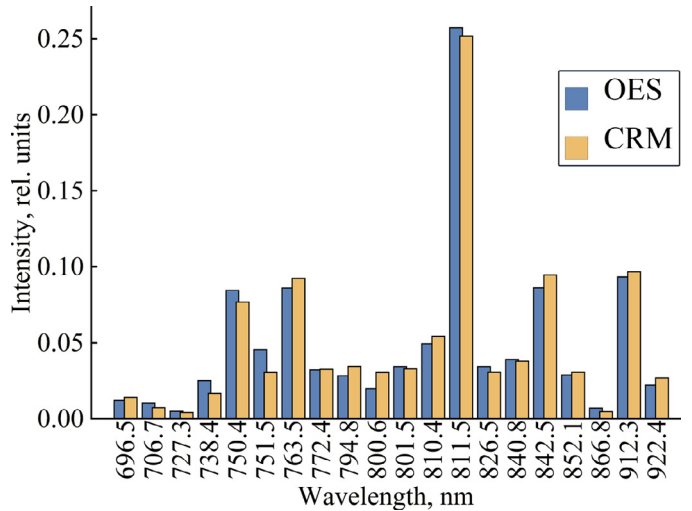
Fig. 3. Comparison of experimental (OES) and theoretical (CRM) spectral line intensities after minimization of merit function (13). Experimental values correspond to emission spectrum of Ar detected in UVN-200MI installation with the following operation parameters: power – 1 kW, gas – Ar, pressure – 0.06 Pa. Minimum of merit function corresponds the following values of variables: $T_g = 493$ K, $\rho = 0.135$ m, $n_e = 3.15 \cdot 10^{16}$ m^{-3}, $\theta_e = 7.37$ eV

as by excitation from ground state of Ar$^+$ ion. The latter process is also called two-step excitation [1] because the atom is ionized first and then the ion is excited. The balance equation determining the population of the state can be written in the following way:

$$
n_e n_{gs} K_+^{ex} + n_e n_+ K_{++}^{ex} = n_+^*/\tau_+, \tag{14}
$$

where n_+ and n_+^* are the number densities of Ar$^+$ ions in ground state and excited state respectively, K_+^{ex} and K_{++}^{ex} are the coefficients of electron-impact excitation from ground state of neutral atom and ion respectively, and τ_+ is the excited state lifetime. Eq. (14) allows determining density n_+ of Ar$^+$ ions in the ground state if other quantities are known.

The density n_+^* of Ar$^+$ ions in the excited state can be estimated from experimental intensity I_+^{OES} of corresponding emission line. On the one hand, relative intensities ($I_+^{CRM}/ \sum_{i'j'} I_{i'j'}^{CRM}$) and ($I_+^{OES}/ \sum_{i'j'} I_{i'j'}^{OES}$) are approximately equal due to minimization of the merit function (13). On the other hand, theoretical value of the intensity I_+^{CRM} is given by the formula similar to (11). Combination of these expressions yields the following equation for n_+^*:

$$
C \frac{hc}{\lambda_+} n_+^* A_+ = I_+^{OES} \frac{\sum_{i'j'} I_{i'j'}^{CRM}}{\sum_{i'j'} I_{i'j'}^{OES}}. \tag{15}
$$

where λ_+ and A_+ are wavelength and transition probability corresponding to the transition.

Solution of Eqs. (14) and (15) requires process specific parameters and values of electron density and temperature. Excitation coefficients K_+^{ex} and K_{++}^{ex} can be calculated by the formula similar to (3). Corresponding excitation cross-sections we deduced from optical ones adopted from Boffard et al. [21] and Zapesochnyi [22]. Quantities τ_+, λ_+ and A_+ referring to the optical transition were adopted from Aparicio et al. [23].

6. Results and discussion

The technique described above was applied to determine parameters of magnetron discharge plasma in UVN-200MI installation. We made experiment at three different values of discharge power while working gas flow rate was sustained at a constant value. Gas pressure was about 0.06 Pa with variations in range of pressure gauge error.

Table 3
Plasma parameters determined by optical and probe methods.

Discharge power, W	OES and CRM					Double probe	
	T_g, K	ρ, m	n_e, m^{-3}	n_+, m^{-3}	θ_e, eV	n_+, m^{-3}	θ_e, eV
1000	493	0.135	$3.15 \cdot 10^{16}$	$3.25 \cdot 10^{16}$	7.37	$9.44 \cdot 10^{17}$	7.86
800	486	0.133	$3.05 \cdot 10^{16}$	$2.61 \cdot 10^{16}$	7.80	$7.59 \cdot 10^{17}$	8.30
500	500	0.150	$2.98 \cdot 10^{16}$	$2.15 \cdot 10^{16}$	9.04	$4.18 \cdot 10^{17}$	9.37

Table 4
Results of stability test regarding experimental data: T_g, ρ, n_e, θ_e.

Parameter	Mean	95% CI	Relative error
T_g	530 K	(250; 1100) K	79%
ρ	0.15 m	(0.07; 0.30) m	78%
n_e	$3.1 \cdot 10^{16}$ m^{-3}	(1.5; 5.4) 10^{16} m^{-3}	61%
θ_e	7.5 eV	(4.9; 11.3) eV	42%

Table 5
Results of stability test regarding experimental data: ρ, n_e, θ_e.

Parameter	Mean	95% CI	Relative error
ρ	0.14 m	(0.10; 0.21) m	39%
n_e	$3.2 \cdot 10^{16}$ m^{-3}	(1.3; 5.6) 10^{16} m^{-3}	69%
θ_e	7.3 eV	(5.6; 9.2) eV	25%

The results of optical and probe diagnostics are presented in Table 3

In order to test stability of the results and estimate uncertainty of determined values, we used a Monte-Carlo method. First, we estimated experimental spectrum standard deviation using several sample spectrums registered under the same conditions. The maximum value of relative standard deviation was about 2.5%. Second, we added normally distributed random noise to the set of experimental relative intensities. Technically, each value was multiplied by random factor, which was normally distributed with mean $\mu = 1$ and standard deviation $\sigma = 0.025$. Then, modified set of intensities was used for determination of plasma parameters. This procedure was repeated several hundred times giving the set of plasma parameters calculated with randomly changed spectrums. Using this set we estimated average values, confidence intervals (CI) and relative errors for all parameters. The calculations was quite extensive and we performed it only for one value of discharge power $P = 1$ kW. Table 4 represents the results of the calculations.

Noticeably, mean values are close to those form Table 3, while CI are quite wide, especially for T_g and ρ. One of the possible ways to narrow CIs is to reduce the number of independent variables. Here we fixed the value of gas temperature T_g because it can be estimated by other means. For example, sample holder temperature is 450 K when magnetron discharge power equals to 1 kW. Another estimate of T_g from gas flow rate, pressure and effective pumping speed gives value about 540 K. The average of these estimates is very close to T_g from Table 3.

The results of stability test for $T_g = 493$ K and ρ, n_e, θ_e as independent variables are shown in Table 5.

It should be pointed out, that errors of θ_e and ρ significantly decreased relative to the previous test, whereas error of n_e even slightly increased. It may be explained by low correlation between n_e and T_g. However, relative errors are still quite high. The probable cause is too simple model. One of the ways to extend it is to use non-maxwellian EEDF, for example bi-maxwellian. The other way may be to account space non-uniformity by introducing different regions of plasma with different parameters.

In addition, we performed similar stability test regarding excitation cross-sections. Instead of experimental relative intensities here
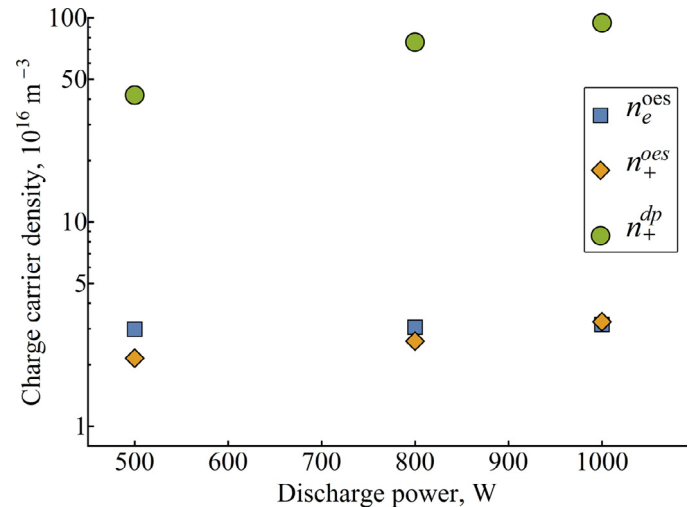
Fig. 4. Plasma charge carrier density vs. magnetron discharge power. Here n_e^{oes} and n_+^{oes} are the electron and Ar$^+$ ion density determined by the optical method; n_+^{dp} is the ion density determined by double probe.
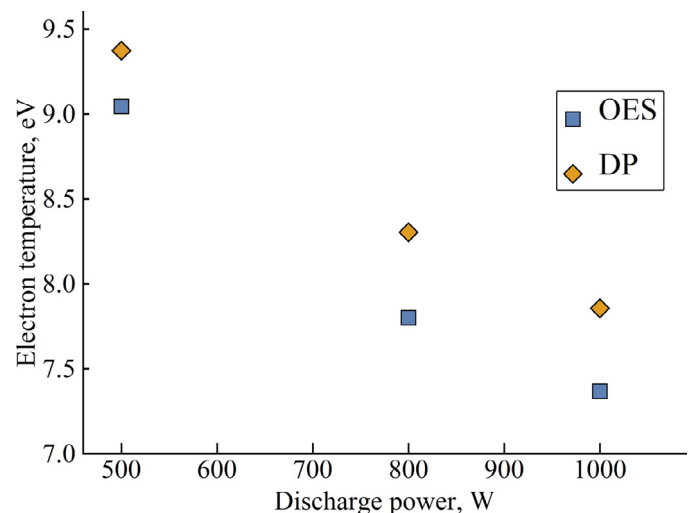
Fig. 5. Electron temperature vs. magnetron discharge power. Here OES and DP denote optical or double probe method respectively.

we multiplied each cross-section by normally distributed random factor with mean $\mu = 1$ and standard deviation σ. All other steps were the same as in previous tests. Table 6 shows results of these calculations for different sets of independent variables and different values of standard deviation of random distribution.

Stability tests show that our method is quite sensitive to variation of cross-sections. Electron temperature is less affected by this variation, while electron density and gas temperature have very wide CI. Anyway, this question needs more detailed research.

The dependences of plasma charge carrier density and electron temperature on magnetron discharge power are shown in Figs. 4 and 5.

Table 6
Results of stability test regarding excitation cross-sections.

	Parameter	Mean	95% CI	Relative error
4 variables $\sigma = 0.05$	T_g	510 K	(200; 1200) K	99%
	ρ	0.14 m	(0.07; 0.32) m	89%
	n_e	$3.1 \cdot 10^{16}$ m^{-3}	(1.4; 5.6) 10^{16} m^{-3}	68%
	θ_e	7.4 eV	(4.4; 12.5) eV	55%
3 variables $\sigma = 0.10$	ρ	0.16 m	(0.08; 0.33) m	80%
	n_e	$3.8 \cdot 10^{16}$ m^{-3}	(0.5; 11.2) 10^{16} m^{-3}	138%
	θ_e	7.3 eV	(4.6; 11.1) eV	45%
3 variables $\sigma = 0.05$	ρ	0.14 m	(0.10; 0.23) m	44%
	n_e	$3.3 \cdot 10^{16}$ m^{-3}	(1.3; 5.6) 10^{16} m^{-3}	86%
	θ_e	7.3 eV	(5.5; 9.5) eV	27%

First, the density of ions determined by the probe and densities of charge carriers determined by OES differ by order of magnitude but exhibit the same behavior with change of discharge power. The difference can be explained by strong plasma non-uniformity as OES gives integral spectrum over all collection volume and the probe may be placed in more dense plasma region. Nevertheless, this question needs further investigation.

Second, the density of electrons and Ar$^+$ ions determined by OES agrees very well, especially at high values of discharge power. This is particularly important because ion density was determined using its own CRM and not relying on quasi-neutrality of the plasma. However, there is a discrepancy between density of electron and ions, and it is increasing with decrease of discharge power. It can be explained by error in determination of 488 nm Ar$^+$ emission line increasing with drop of discharge power. This error may be caused by necessity of extraction of comparatively weak 488 nm Ar$^+$ emission line from superposition of residual gases lines. For example, there is atomic hydrogen in the chamber with 486 nm emission line brighter than that of Ar$^+$. Nevertheless, density of ions is inside CI for electron density in all cases.

Finally, the electron temperature determined by both methods agrees quite well and differs by no more than 10 per cent, which is less that our estimate of error for electron temperature. Also, electron temperature values are higher than usual 3–5 eV for other magnetron discharges. It may be explained by relatively low pressure in our case.

7. Conclusion

In this work we proposed a method of determining temperature and density of electrons in plasma based on minimization of difference between relative intensities of Ar spectral lines given by experiment and calculated by CRM. The method was applied for study of parameters of magnetron discharge plasma in laboratory installation UVN-200MI for reactive sputter deposition. Also, we determined Ar$^+$ ions density using simple CRM accounting one-step and two-step excitation.

To test the stability of results, we performed Monte-Carlo calculations with random variation of experimental spectrum and estimated confidence intervals and errors for plasma parameters. In case of four independent variables T_g, ρ, n_e, θ_e relative error was quite high. Independent estimate of T_g and calculation for three variables gave significantly lower error for electron temperature and plasma characteristic length. In addition, we performed stability tests regarding variation of excitation cross-sections. Electron temperature is less affected by this variation, while electron density has quite large error.

The results were verified by double probe plasma diagnostics. Plasma charge carrier density determined by optical method is lower by an order of magnitude than density determined by probe and it can be explained by strong non-uniformity of plasma. The density of ions determined by OES agrees very well with electron density especially at high values of discharge power. Both methods give similar values of electron temperature with maximal difference not exceeding 10 per cent.

References

[1] J.B. Boffard, C.C. Lin, C.A. DeJoseph, Application of excitation cross sections to optical plasma diagnostics, J. Phys. D 37 (2004) R143–R161.

[2] V.M. Donelly, Plasma electron temperatures and electron energy distributions measured by trace rare gases optical emission spectroscopy, J. Phys. D 37 (2004) R217–R236.

[3] S. Iordanova, I. Koleva, Optical emission spectroscopy diagnostics of inductively-driven plasmas in argon gas at low pressures, Spectrochim. Acta B. 62 (2007) 344–356.

[4] X.-M. Zhu, Y.-K. Pu, Optical emission spectroscopy in low-temperature plasmas containing argon and nitrogen: determination of the electron temperature and density by the line-ratio method, J. Phys. D 43 (2010) 403001 (24pp).

[5] J.B. Boffard, R.O. Jung, C.C. Lin, A.E. Wendt, Measurement of metastable and resonance level densities in rare-gas plasmas by optical emission spectroscopy, Plasma Sources Sci. Technol. 19 (2010) 065001 (15pp).

[6] X.-M. Zhu, Y.-K. Pu, Y. Celik, S. Siepa, E. Schungel, D. Luggenholscher, U. Czarnetzki, Possibilities of determining non-Maxwellian EEDFs from the OES line-ratios in low-pressure capacitive and inductive plasmas containing argon and krypton, Plasma Sources Sci. Technol. 21 (2012) 024003 (11pp).

[7] R.H. Huddlestone, S.L. Leonard, Plasma Diagnostic Techniques, Academic Press, New York, 1965.

[8] M.E. Konischev, O.S. Kuzmin, A.A. Pustovalova, N.S. Morozova, K.E. Evdokimov, R.A. Surmenev, V.F. Pichugin, M. Epple, Structure and properties of Ti–O–N coatings produced by reactive magnetron sputtering, Russ. Phys. J. 56 (2014) 1144–1149.

[9] K.E. Evdokimov, M.E. Konishchev, S. Chzhilei, V.F. Pichugin, Langmuir probe study of reactive magnetron discharge plasma in a three-component gas atmosphere, Instrum. Exp. Tech. 59 (2016) 816–821.

[10] A. Brockhaus, C. Borchardt, J. Engemann, Langmuir probe measurements in commercial plasma plants, Plasma Sources Sci. Technol. 3 (1994) 539–544.

[11] R.K. Gangwar, L. Sharma, R. Srivastava, A.D. Stauffer, Argon plasma modeling with detailed fine-structure cross sections, J. Appl. Phys. 111 (2012) 053307.

[12] NIST Atomic Spectra Database, http://www.nist.gov/pml/data/asd.cfm, (21.12.2016).

[13] M.A. Lieberman, A.J. Lichtenberg, Principles of Plasma Discharges and Materials Processing, Wiley-Interscience, Hoboken, NJ, 2005.

[14] O. Zatsarinny, Y. Wang, K. Bartschat, Electron-impact excitation of argon at intermediate energies, Phys. Rev. A. 89 (2014) 022706.

[15] K. Bartschat, V. Zeman, Electron-impact excitation from the (3p⁵4s) metastable states of argon, Phys. Rev. A 59 (1999) R2552.

[16] L.C. Pitchford, L.L. Alves, K. Bartschat, S.F. Biagi, M.C. Bordage, A.V. Phelps, C.M. Ferreira, G.J.M. Hagelaar, W.L. Morgan, S. Pancheshnyi, V. Puech, A. Stauffer, O. Zatsarinny, Comparisons of sets of electron–neutral scattering cross sections and swarm parameters in noble gases: I. Argon, J. Phys. D 46 (2013) 334001 (19pp).

[17] J.B. Boffard, R.O. Jung, C.C. Lin, A.E. Wendr, Measurement of metastable and resonance level densities in rare-gas plasmas by optical emission spectroscopy, Plasma Sources Sci. Technol. 18 (2009) 035017 (11pp).

[18] M. Asgar Ali, P.M. Stone, Electron impact ionization of metastable rare gases: He, Ne and Ar, Int. J. of Mass Spectr. 271 (2008) 51–57.

[19] H. Deutsch, K. Becker, A.N. Grum-Grzhimailo, K. Bartschat, H. Summerse, M. Probst, S. Matt-Leubner, T.D. Märk, Calculated cross sections for the electron-impact ionization of excited argon atoms using the DM formalism, Int. J. of Mass Spectr. 233 (2004) 39–43.

[20] B.M. Smirnov, Excited Atoms, Energoizdat, Moscow, 1982.
[21] J.B. Boffard, B. Chiaro, T. Weber, C.C. Lin, Electron-impact excitation of argon: optical emission cross sections in the range of 300–2500 nm, At. Data Nucl. Data Tables 93 (2007) 831–863.

[22] I.P. Zapesochnyi, A.I. Imre, A.I. Dashchenko, V.S. Vukstich, F.F. Danch, V.A. Kel'man, Experimental investigation of the excitation of Ar II and Kr II in electron-ion collisions, Sov. Phys. JETP 36 (1973) 1056.
[23] J.A. Aparicio, M.A. Gigosos, S. Mar, Transition probability measurement in an Ar II plasma, Phys. B 30 (1997) 3141–3157.